



# Impact of potential flood on riverbanks in extreme hydro-climatic events, NW Himalaya

Yaspal Sundriyal<sup>1</sup> · Vipin Kumar<sup>2</sup> · Firoz Khan<sup>1</sup> · Mohit Kumar Puniya<sup>3</sup> · Sameeksha Kaushik<sup>1</sup> · Neha Chauhan<sup>1</sup> · Dharendra Singh Bagri<sup>1</sup> · Naresh Rana<sup>4</sup>

Received: 1 December 2022 / Accepted: 3 April 2023  
© Springer-Verlag GmbH Germany, part of Springer Nature 2023

## Abstract

Floods are becoming more frequent in Himalaya, particularly in the NW Himalaya, and have been related to the increasing impact of changing climate. Uttarakhand in the NW Himalaya has witnessed 2 major flood events in the last decade that killed more than 6000 people. This study is an attempt to explore the impact of potential flood on a riverbank slope in Uttarakhand, NW Himalaya. The response of this riverbank slope during extreme rainfall is also explored in terms of stability and debris flow runout. Therefore, we evaluated the riverbank slope stability and the runout extent of its material to understand the slope response during extreme rainfall. Flood simulation was also performed to determine the potential flood impact on the riverbank slope. Results revealed that the slope material at the exposed fluvial sequence and slope toe might displace forward ~0.12–0.4 m. The potential debris flow from the slope may impact the retaining wall supporting the slope with a pressure up to 150 k Pa. The potential flood may strike the riverbank with a velocity and stream power of  $10 \pm 2$  m/s and  $0.2 \pm 0.1$  M N/m-s, respectively, which is about three times higher than the approximated resistance of the retaining wall.

**Keywords** Flood · Climate change · Debris flow · Slope stability · Riverbank · Himalaya

## Introduction

Recent studies from Himalaya and other mountain systems have noted various implications of changing climate in the form of elevation-dependent warming, extreme rainfalls, and increased surface runoff (Bhutiyan et al. 2010; Shekhar et al. 2010; Dimri et al. 2020; Kumar et al. 2021a). Such a change in these climatic parameters is noted to be the primary cause of frequent snow avalanches, landslides, cloud bursts, and floods particularly in Himalaya (Dhakal 2014; Gupta et al. 2017; Kumar et al. 2018, 2021b; Dimri et al. 2021; Sundriyal et al. 2023). Notably, the NW part of the Himalaya has been subjected to frequent extreme hydro-climatic events, debris flows, cloud bursts, and floods in the last decade that have

caused the social and economic loss of ~6000 lives and more than 1 billion USD, respectively, within a decade (Chopra 2014; Martha et al. 2015; Sati and Kumar 2022). The potential loss in future associated to similar events can be approximated from the fact that only two extreme events; June 16–17, 2013 flood and February 7, 2021 flash flood have resulted in the aforementioned socio-economic loss (Sundriyal et al. 2015; Rana et al. 2021). Such floods have been observed to affect the landform processes along their downstream flow in the form of riverbank erosion, generation of new landslides, and reactivation of old landslides (Martha et al. 2015; Sundriyal et al. 2015). In this study, we are exploring the aspect of riverbank erosion in case of potential flood, which is still a less studied phenomenon despite the risk associated with such riverbanks, particularly if the riverbanks are composed of fluvial sediments.

Though the riverbank stabilization using various slope stabilization measures has been a common practice (Gray and Sotir 1996; Goldsmith et al. 2013), the sustainability of such measure has been ineffective owing to a poor understanding of slope response and impact of potential flood (Thorne and Tovey 1981; Baker 1987; Van der Wal 2020; Das and Samanta 2022). By evaluating the slope response

✉ Vipin Kumar  
v.chauhan777@gmail.com

<sup>1</sup> Department of Geology, HNB Garhwal University, Srinagar, India

<sup>2</sup> Department of Geology, Doon University, Dehradun, India

<sup>3</sup> National Geotechnical Facility, Dehradun, India

<sup>4</sup> Department of Geology, University of Delhi, Delhi, India

in terms of stability under different natural/anthropogenic conditions and simulating the potential flood impact, the response of the riverbank and/or stabilization measures protecting such banks can be understood. Continuum modelling-based slope stability evaluation has been among the most widely used approaches for complex slope geometry problems like riverbanks (Griffiths and Lane 1999; Jing 2003; Jamir et al. 2017; Kumar et al. 2021b). Since the possibility of debris flows on the riverbanks consisting of loose fluvial sediments cannot be ignored in case of extreme rainfall, debris flow runout analysis is also an integral part of understanding the slope response. Such runout analysis method could be classified into empirical/statistical and dynamical categories (Rickenmann 2005). Dynamic models have been relatively more realistic due to the flexibility in rheology, reference frame, and entrainment. Among different runout prediction approaches, dynamic model based Flo-2D (O'Brien et al. 1993), MassMov2D (Beguiria et al. 2009), rapid mass movement simulation (RAMMS) (Christen et al. 2010), and r.avaflow (Pudasaini and Mergili 2019) have been relatively more rational for reconstruction and prediction (Rickenmann and Scheidl 2013). Though the different runout numerical models have different advantages and limitations, Voellmy rheology (Voellmy 1955; Salm 1993)-based RAMMS has been used widely owing to the inclusion of rheological, multiple release area, temporal setting, quick and effective visualization, and entrainment rate flexibility (Christen et al. 2010; Kumar et al. 2021a, b).

Apart from the stability and runout aspect of riverbank slope, impact of regional hydro-climatic processes like flood is also required to explore. Flood simulation using the 2D hydrodynamic models has been the most widely used approach due to parameterization capability, inclusion of climatic variables, lateral inundation understanding, and flexible time steps (Teng et al. 2017 and reference therein). Though the 3D hydrodynamic models have also been in use in the last decade, computational feasibility, high order turbulence, and limited understanding of vertical layers over a larger area make them a less preferred choice over the 2D models (Alcrudo 2002; Teng et al. 2017). Though more than 20 commercial and open-access software currently offer 2D hydrodynamic flood simulation, each has certain advantages and limitations that are changing with time. Among these softwares, HEC-RAS software has been used widely owing to finite volume approach, open access, the flexibility of equation solver, and time step (HEC-RAS v.6).

In the present study, we are discussing a riverbank situated at the right bank of Alaknanda River valley, Uttarakhand, NW Himalaya. The June 16–17, 2013 flood in Alaknanda valley had carved out  $\sim 95,000 \text{ m}^3$  (“Fieldwork, laboratory analyses, and unmanned air vehicle (UAV) mapping” section) slope mass of this riverbank that used to support roads and other infrastructure facilities until the flood

stroke. Later in the year 2016–2017, to minimize the slope toe erosion and protect the remaining vulnerable riverbank from future floods, a  $\sim 537\text{-m}$ -long retaining wall was constructed at the cost of USD  $\sim 1.24$  million. Within 3–4 years, this wall has collapsed at two places and hence poses a socio-economic risk in case of another flood. The present study is an attempt to evaluate the response of this exposed riverbank in case of local (slope stability/debris flow) as well as regional processes (flood) that might impact the riverbank and pose associated infrastructure risk.

## Study area

The study area, i.e., riverbank slope, is situated at latitude  $30^\circ 13' 21.8'' \text{ N}$  and longitude  $78^\circ 48' 20.3'' \text{ E}$  along the Alaknanda River, Uttarakhand, NW Himalaya (Fig. 1). The slope that has an azimuth of  $73^\circ\text{--}74^\circ \text{ N}$  with  $22\text{--}27^\circ$  inclination is composed of unconsolidated overburden comprising fluvial sediments underlain by Phyllite rock mass.

The vulnerability of the study area can be understood from the fact that it is situated within 100 km from the origin and epicenter of a major flood and major earthquakes in the region. The four known major flood events in the region are as follows: August 24–26, 1894, July 20, 1970, June 16–17, 2013, and February 7, 2021 that resulted in widespread loss of lives and property (Ziegler et al. 2014; Sundriyal et al. 2015), whereas three major earthquakes are September 1, 1803 ( $M_w$  7.8), October 20, 1991 ( $M_w$  6.8), and March 29, 1999 ( $M_w$  6.6) (Kayal 1996; Pandey et al. 2001; Bilham 2019).

Notably, all these major events occurred in the vicinity of the Main Central Thrust (MCT). The position of the MCT fault has been attributed to the Main Himalayan Thrust (MHT) ramp structure in the region that allows strain accumulation at shallow depths and hence the occurrence of frequent and major earthquakes (Bilham 2019). The MCT also acts as an orographic barrier to saturated winds of the Indian summer monsoon (ISM) and western disturbance (WD), resulting in relatively higher precipitation in the orographic front (Gadgil et al. 2007; Hunt et al. 2018). Notably, increasing rainfall, surface runoff, and surface radiative temperature during the years 1991–2021 in the orographic barrier increase the possibility of another flood/ice-rock avalanche that might impact the study area situated downstream (Fig. 2a–e). The daily rainfall is also noted to increase in the upstream and study area, particularly after the year 2010 (Fig. 2f, g).

The impact of the last major flood, i.e., June 16–17, 2013 was also noted in the river discharge at various measuring points along the Alaknanda valley (Fig. 3a–e). Apart from this flood, the upstream region of the study area has been subjected to 2 major hydro-climatic events (Fig. 3a). This flood killed  $> 6000$  people and carved out  $\sim 0.95 \text{ M m}^3$  mass

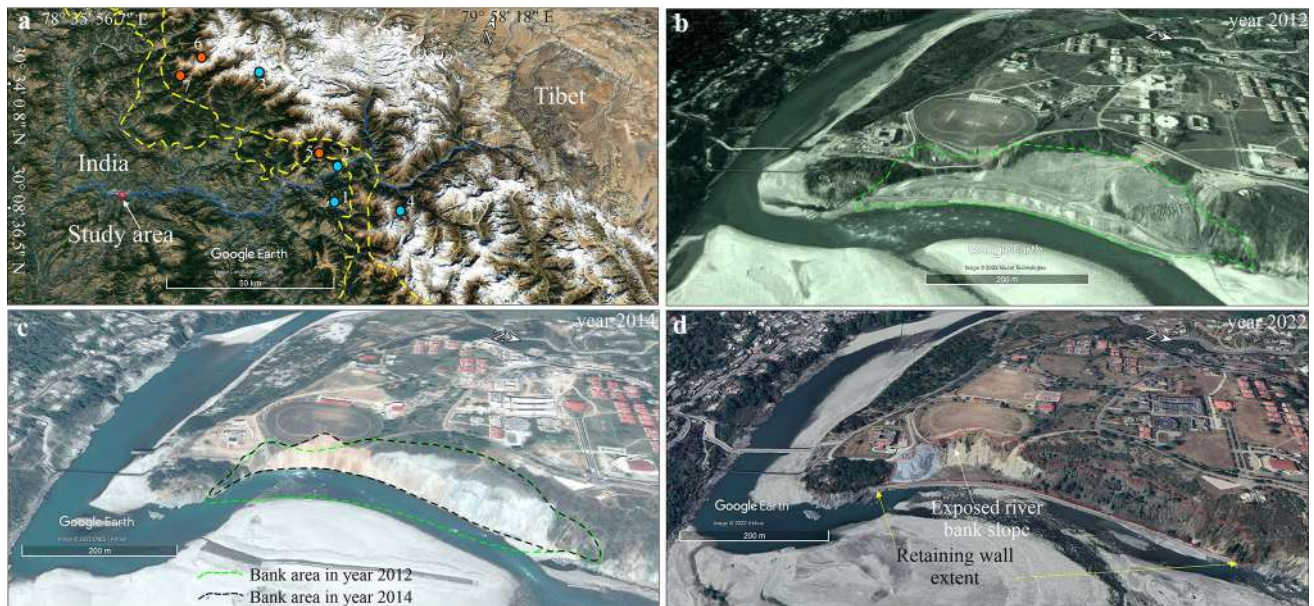


**Fig. 1** Study area. **a** Position of study area. Points 1 (August 24–26, 1894), 2 (July 20, 1970), 3 (June 16–17, 2013), and 4 (February 7, 2021) refer to major flood/landslide/cloud burst events, and points 5 (March 29, 1999, Mw 6.6), 6 (September 1, 1803, Mw 7.8), and 7 (October 20, 1991, Mw 6.8) refer to major earthquake events. Yellow

dashed lines represent main central thrust fault zone. **b** Study area in year 2012. **c** Study area in year 2014. Note the exposed slope on right bank, carved out by June 2013 flood. **d** Study area (exposed riverbank slope) in year 2022 comprising 537 m long retaining wall constructed in year 2016–2017. Image source: Google Earth

from the riverbank slope, which involved infrastructure loss in the form of roads and sports stadium.

Details of the carved-out volume are mentioned in the “Fieldwork, laboratory analyses, and unmanned air vehicle (UAV) mapping” section. Reconstructed road, sports stadium, temple, and other buildings situated on this fluvial sequence slope comprising gravelly sand and pebble-cobble layer are still at risk in view of another major flood event (Fig. 4). Though a 537-m-long retaining wall comprising front rows of concrete blocks and back row of gabion walls was constructed in the year 2016–2017 to protect this riverbank slope from further flood erosion, it has collapsed at two places even without any flood since construction (Fig. 4b). Localized slope failure activities along the riverbank are also noted that may aggravate the situation in case of further saturation of loose material by rainfall or toe cutting by another major flood (Fig. 4d, e).

## Methodology

The possibility of another major flood event in the study area cannot be denied because of the history of floods and associated high river discharge. We understand that the retaining wall, constructed to protect the riverbank slope from further erosion, is subjected to local and regional impacts that might damage it completely, hence making riverbank slope and roads/other infrastructure (buildings) vulnerable again. For

local impact evaluation, slope stability analysis and debris flow analysis were performed, whereas flood simulation study was performed for regional impact evaluation. Details of these analyses are as follows;

### Fieldwork, laboratory analyses, and unmanned air vehicle (UAV) mapping

Fieldwork involved mapping of the retaining wall and soil sampling. The dimension (volume) of concrete and gabion blocks of retaining wall was measured (Fig. 5) in the field to calculate their mass (kg) and, hence, resistance (N/m) toward external forces (debris flow pressure and/or flood stream power).

The density of concrete and gabion wall blocks is based on IS 14458 (Part 2) 1997, Reaffirmed 2002, and IRC: SP: 116–2018. The gabion block and concrete block, with their respective masses of ~15,147 kg (or 148541 N) and ~1800 kg (or 17651 N), offer ~166,193 N/m (or 0.16 M N/m) force against potential flood or debris flow pressure. This force or resistance, however, decreases to (166,193–17651 N/m) 0.14 M N/m at two places where concrete blocks are collapsed.

The slope stability analysis, which was performed on this riverbank slope, required various input parameters of soil and rock, among which soil parameters were determined in the National Geotechnical Facility (NGF), Dehradun, India for various input parameters (Supplementary Table 1). The

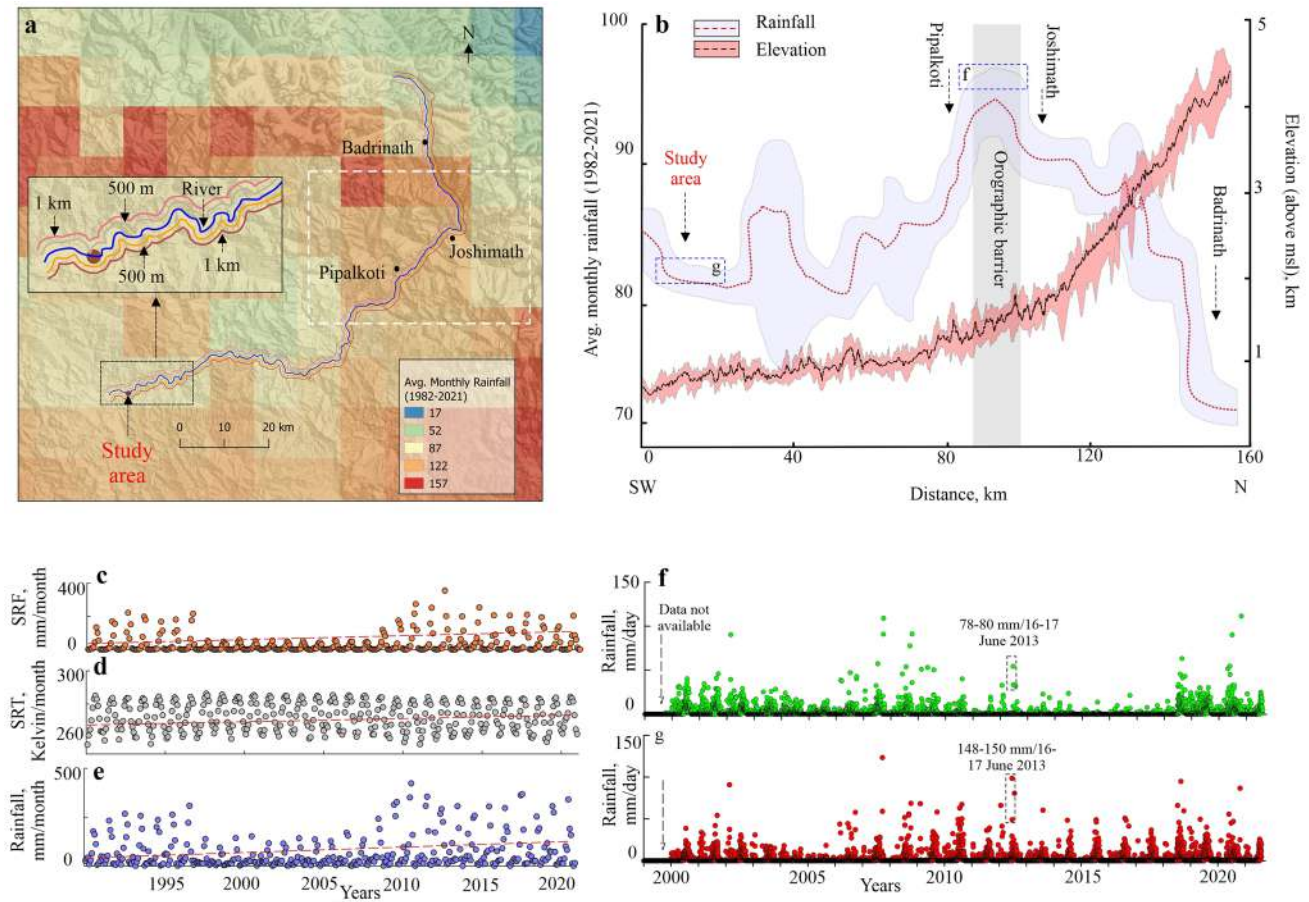


**Fig. 2** Climatic pattern. **a** Location of the study area in spatially varying avg. monthly rainfall (1982–2021) map underlain by ALOS PALSAR DEM (accessed from [www.vertex.daac.asf.alaska.edu](http://www.vertex.daac.asf.alaska.edu) on February 2, 2022). 500-m and 1-km buffer areas on both sides of river were used to extract rainfall and elevation profiles, as shown in (b). White dashed area represents the region used to extract time series climate data (1991–2021) of rainfall, surface radiative temperature (SRT), and

surface runoff (SRF), shown in (c), (d), and (e). **f–g** Daily rainfall data at orographic barrier and study area, respectively. Climate data source except in (f)–(g): FLDAS\_NOAH01\_C\_GL\_M model (McNally 2018). Spatial resolution:  $0.1^\circ$  ( $\sim 10$  km). Data source of (f–g): GPM IMERG Final Precipitation (Huffman et al. 2020) Spatial resolution:  $0.01^\circ$  ( $\sim 1$  km)

soil samples were tested for grain size analysis (IS: 2720-part 4–1985), density (IS: 2720-part 4–1980), UCS test (IS: 2720-part 10–1991), and direct shear test (IS: 2720-part 13–1986). In the direct shear test, soil samples were sheared under constant normal stress of 50, 100, and 150  $\text{kN/m}^2$ . The UCS soil test was performed under three different movement rates, i.e., 1.25, 1.50, and 2.5 mm/min.

The DJI Phantom 4 RTK UAV (having  $\pm 0.1$  m horizontal and vertical accuracy) was used to prepare the current topography and hence to extract the 2D slope section for the slope stability analysis and debris flow analysis (Fig. 6). Drone height was maintained at 100 m to achieve the  $\sim 2.7$  cm/pixel accuracy as per H/36.5 equation (<https://www.dji.com/phantom-4-rtk/info>, retrieved on 03/07/2022). H refers to aircraft altitude relative to the shooting scene. Drone images were processed to prepare the DSM and DTM using Pix4DMapper (v 4.7.5) software (Pix4D SA, Switzerland). The volume of the slope

material carved out by June 16–17 flood was determined by calculating the riverbank slope area's difference in 2012 and 2014 (Fig. 1b, c) in QGIS (v.3.14). The ALOS PALSAR DEM (accessed from [www.vertex.daac.asf.alaska.edu](http://www.vertex.daac.asf.alaska.edu), on February 2, 2022) was used to extract the volume in this area. An uncertainty of 2.0% was noted between known distances/area (field measurement) and measured ones in Google Earth. The riverbank had an approximate area of  $52,529 \pm 1050$  and  $29,386 \pm 587$   $\text{m}^2$  in 2012 and 2014, respectively (Fig. 1c).

### Slope stability analyses

The finite element method (FEM)-shear strength reduction (SSR)-based slope stability analysis was performed to infer the total displacement (TD) using the RS2 v.11.012 software. The boundary conditions with the restraining X and

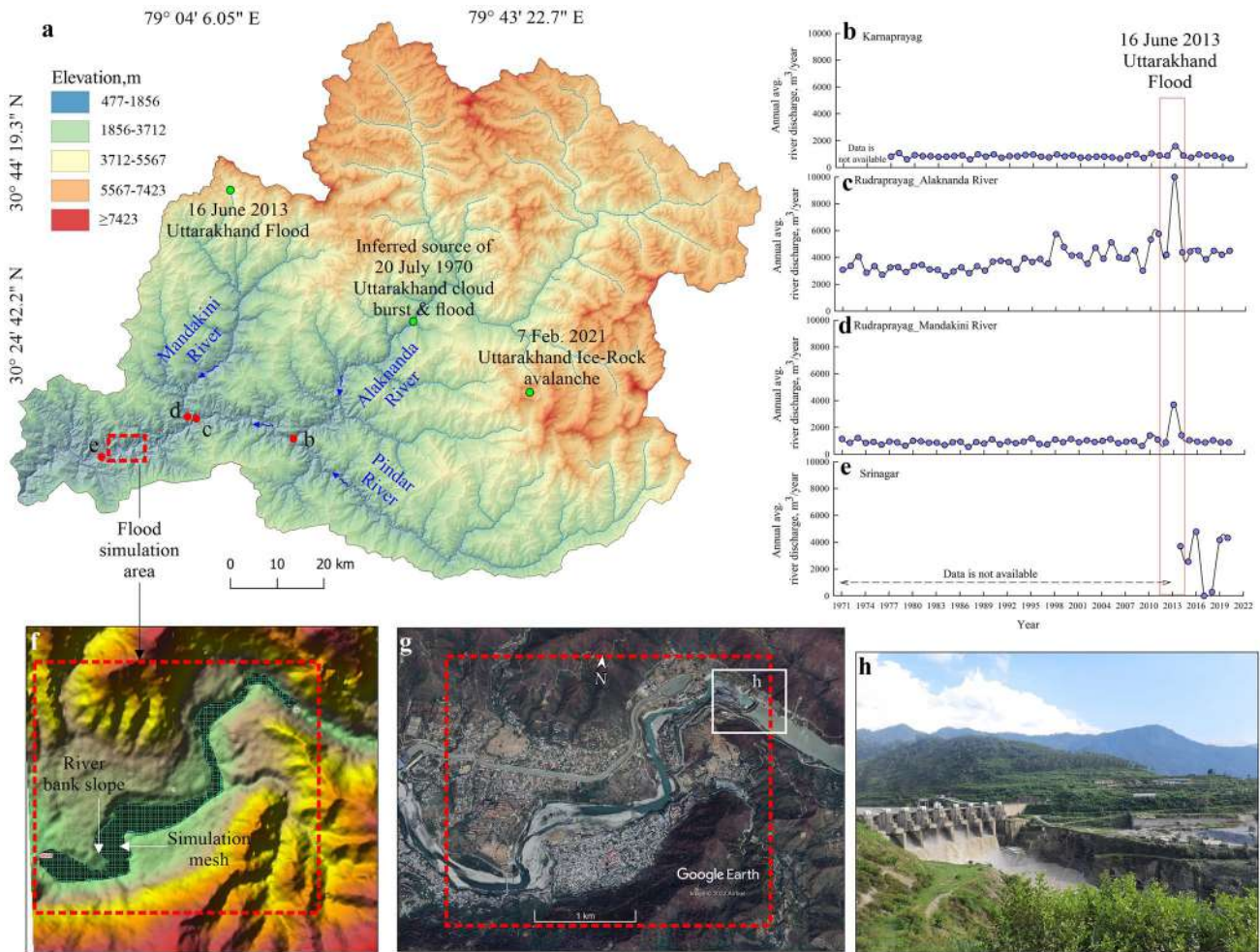


**Fig. 3** River discharge. **a** Locations of flood simulation area. June 16, 2013, July 20, 1970, and February 7, 2021 are major hydro-climatic events upstream of the study area. **b–e** River discharge (annual average) measurement points. The red highlighted area represents peak discharge during June 2013 flood. Data source: Himalaya Ganga Divi-

sion, Central Water Commission, Uttarakhand, India. **f–g** Flood simulation area marked on ALOS Palsar DEM and Google Earth imagery, respectively. **h** Hydropower project reservoir, which is considered upper boundary (source of discharge) for flood simulation

Y movements were applied to the base and back, whereas the front face of the slope sections was kept free for the movement (Fig. 7a–c). Notably, If *x* and *y* movements are not restrained at the base and back, displacement of front face cannot be reliable because the model itself would not be stationary. In situ field stress was adjusted in view of dominant forces, i.e., compressional regime, by using the value of the coefficient of earth pressure ( $k$ ) = (horizontal field stress)  $\sigma_h$  / (vertical field stress)  $\sigma_v = 1.5$ . The compressional regime was taken in view of the vicinity of the north Almora thrust (NAT) fault (Supplementary Fig. 1). Analysis was performed in two stages: without water ponding and with water ponding. Water ponding was applied as per the guidelines for retaining wall construction along the waterbody (<https://www.rocsience.com/help/rs2/tutorials/excavations/retaining-wall>). Water ponding condition was used because

the toe of the riverbank slope and part of the retaining wall remain submerged in the river water during high discharge season (July–October). Rainfall infiltration was applied in both stages. Rainfall infiltration (RF) is based on extreme rainfall (~98 mm/24 h) events on June 16, 2013 in the region (Fig. 2g) and the possibility of recurrence.

The soil and rock mass were used in the FEM analysis through Mohr–Coulomb (M-C) failure criterion (Coulomb 1776; Mohr 1914) and generalized Hoek–Brown (GHB) criterion (Hoek et al. 1995), respectively. The soil behavior was assumed as undrained in view of field conditions. Water bulk modulus was taken as 2.18 GPa (The study area has an avg. annual temperature of  $24 \pm 2$  °C). The degree of saturation and permeability were determined using the Van Genuchten function. The value of input parameters for this function was based on empirical studies of Schroth et al. (1998).

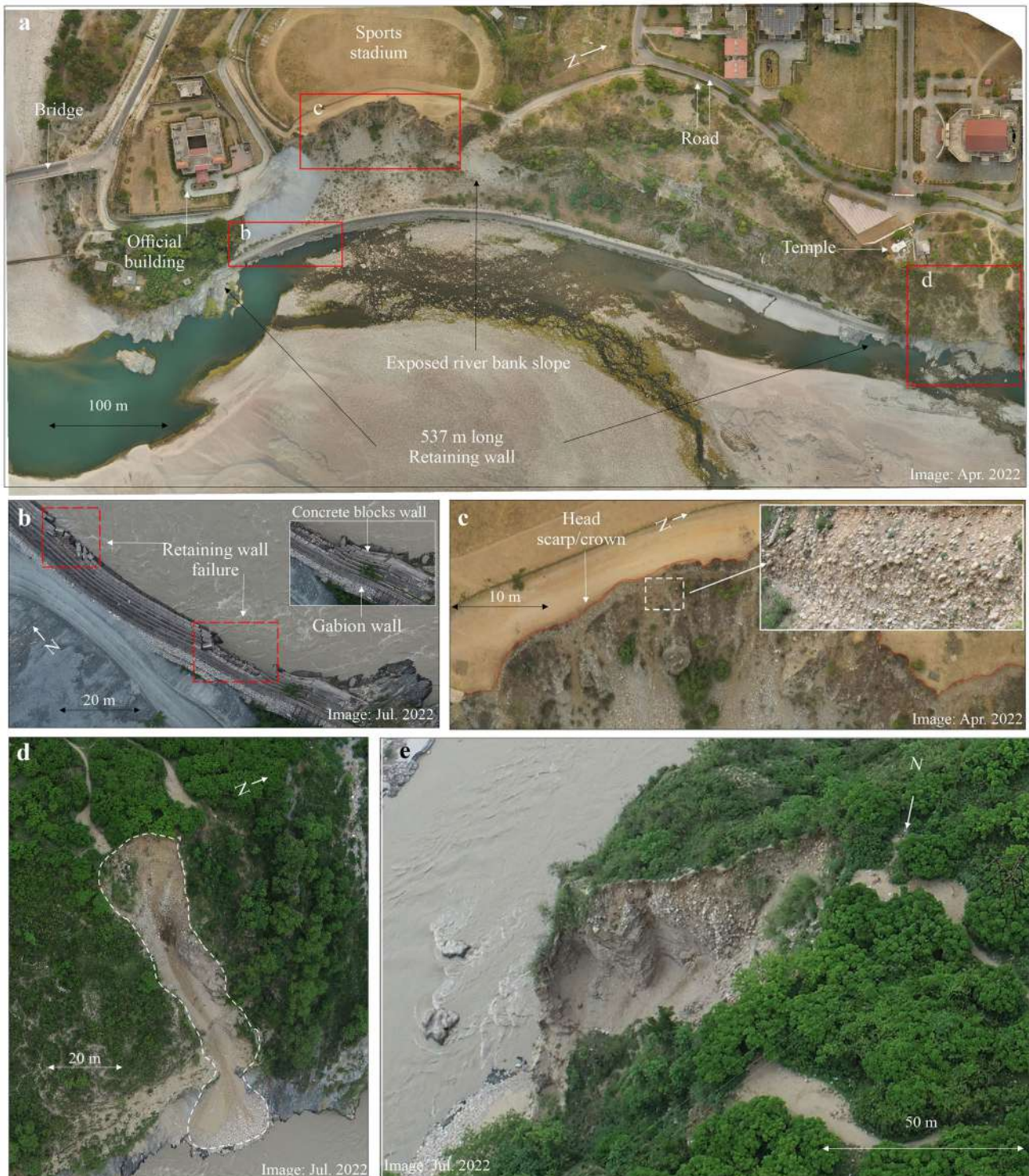


**Fig. 4** Field pictures of study area. **a** Bird view of exposed riverbank slope retaining wall and risk elements (road, buildings, stadium, and temple). **b** Collapse in the retaining wall. **c** Composition of slope, i.e., fluvial sediments. **d** Slope failure development. **e** Side view of slope failure

The joint between the retaining wall and fluvial sediments (Fig. 7c) was applied through Barton–Bandis (B-B) slip criterion (Barton and Choubey 1977; Barton and Bandis 1990). Plane strain triangular elements having 6 nodes were

used through the graded mesh in the models. Details of input parameters are present in Supplementary Table 1. To find out the relative influence of main input parameters on the displacement, a sensitivity analysis was also performed.

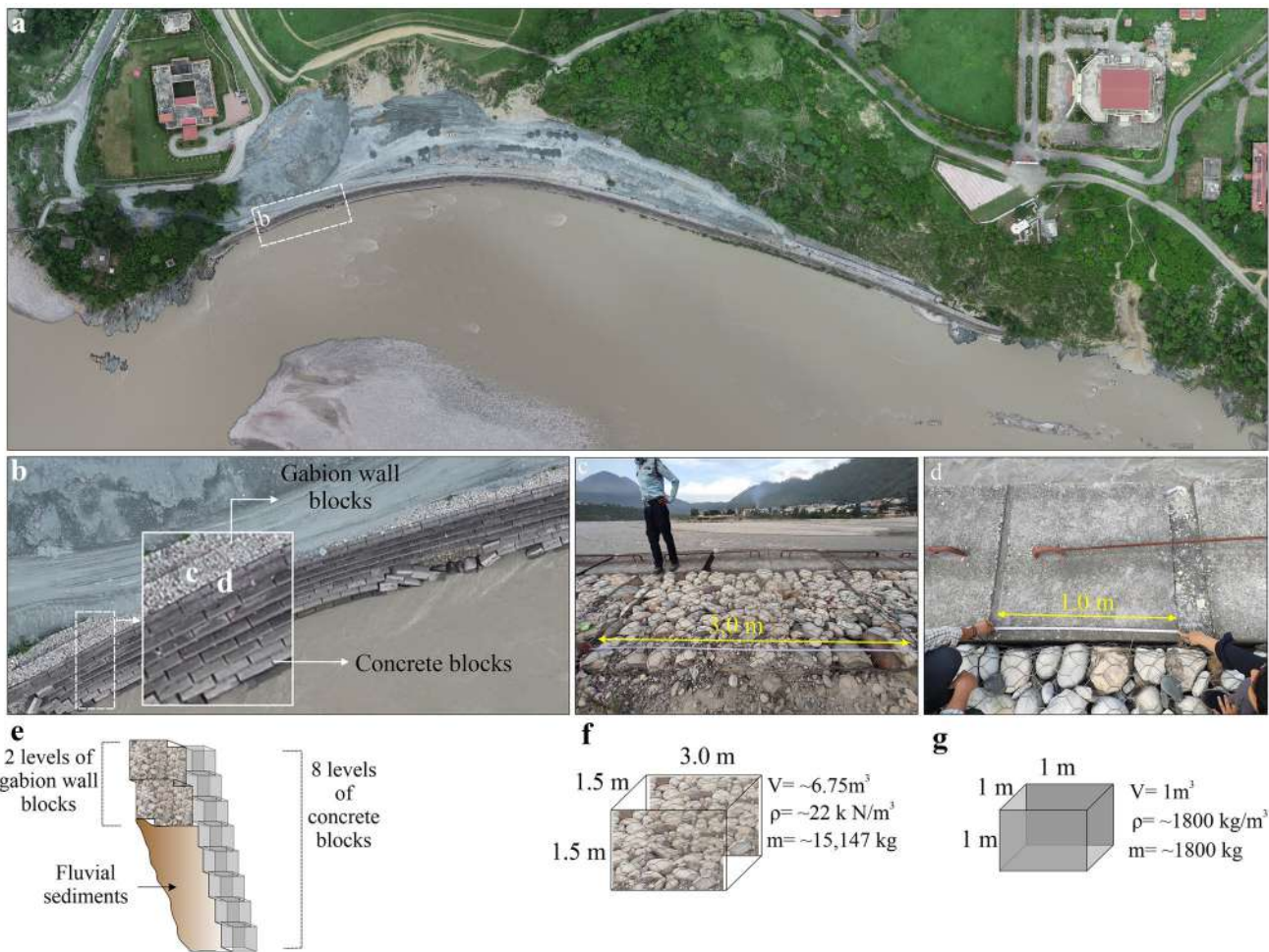


**Fig. 5** Retaining wall description. **a** Bird view of exposed riverbank slope along with retaining wall. **b–d** Field measurement of concrete and gabion blocks of retaining wall. **e–g** Dimension of concrete and

gabion blocks. Density of concrete blocks and gabion blocks are based on IS 14458 (part 2) 1997, Reaffirmed 2002, and IRC SP:116 (2018)

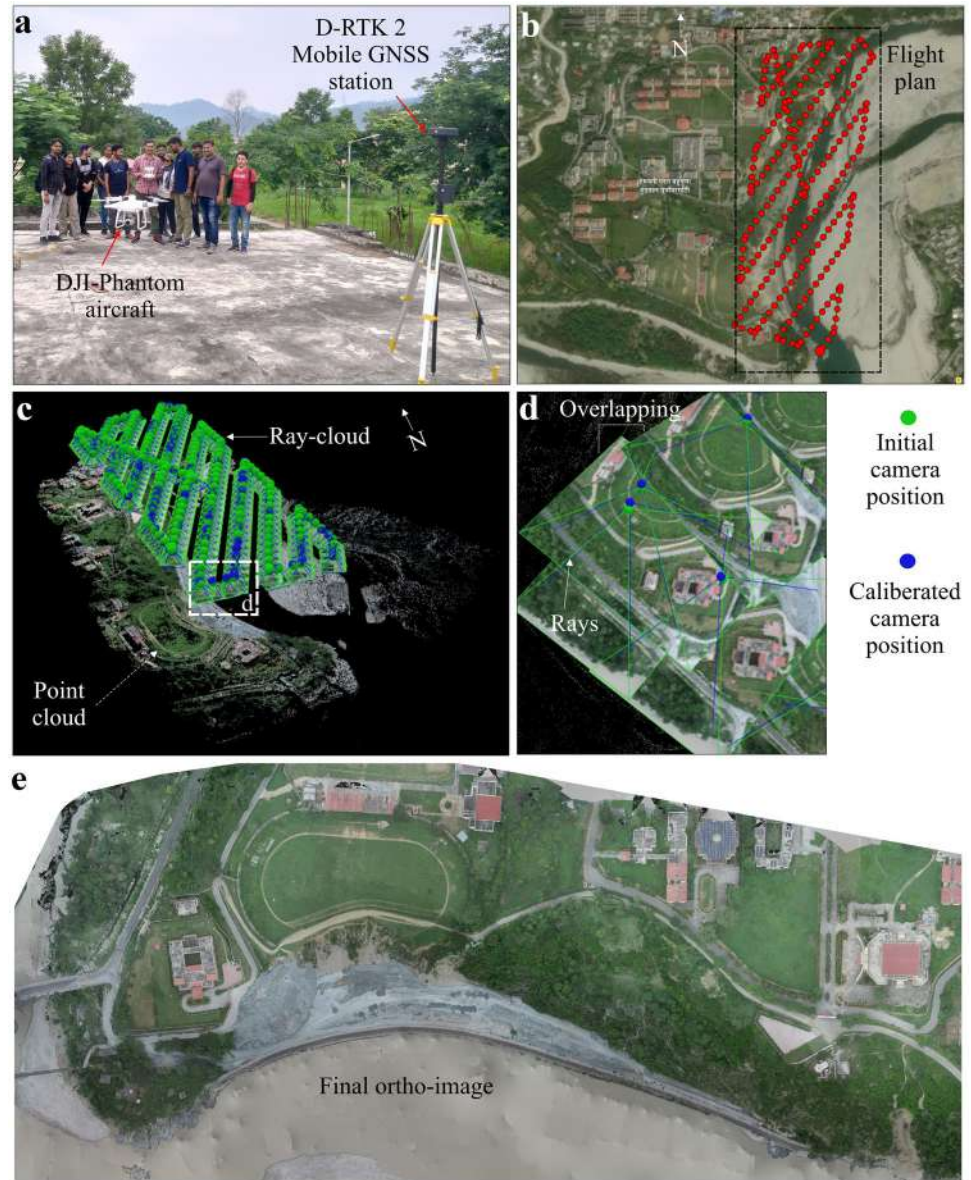
### Run-out simulation

Due to its loose material (fluvial sediments) composition and previous response during the June 2013 flood, the riverbank slope is more prone to rainfall-induced slope failures, particularly in the form of debris flows. Such debris flows can initiate either by increased pore pressure or runoff involving entrainment, as Godt and Coe (2007) noted. The Voellmy friction law-based model was simulated using the rapid mass movement simulation (RAMMS) software to ascertain the outreach of such potential debris flow during an extreme rainfall event. The RAMMS divides the frictional resistance into dry-Coulomb-type friction ( $\mu$ ) and viscous-turbulent friction ( $\xi$ ) (Christen et al. 2010). The frictional resistance  $S$  (Pa) is thus

$$S = \mu N + (\rho g u^2) / \xi \tag{1}$$

where  $N = \rho h g \cos(\phi)$ .  $N$  = normal stress on the running surface,  $\rho$  = density,  $g$  = gravitational acceleration,  $\phi$  = slope angle,  $h$  = flow height, and  $u = (u_x, u_y)$ , consisting of the flow velocity in the  $x$ - and  $y$ -directions, generally, the values for  $\mu$  and  $\xi$  parameters are achieved using the reconstruction of real events through simulation and subsequent comparison between dimensional characteristics of real and simulated event. However, the toe of riverbank slope and previous flow material has been altered after the retaining wall construction; hence, there is an uncertainty in the reconstruction of the volume of previous flow events. Therefore,  $\mu$  and  $\xi$  along with depth and density are taken by sensitivity analysis in view of the topography of slope and run-out path, slope material, and based on previous studies/models (Hürlimann et al. 2008; Rickenmann and Scheidl 2013; RAMMS v.1.7.0). Details of input parameters and their source are presented in Supplementary Table 2. Slope material depth levels were

**Fig. 6** UAV- DJI Phantom 4 RTK based mapping. **a** D-RTK-2 Mobile GNSS station setup. **b** Flight plan in study area. **c, d** Image processing in Pix4D software. **e** Final ortho-image



approximated based on field observation (Supplementary Fig. 2). Further, details of the governing equations of debris flow simulation can be accessed in Kumar et al. (2021a).

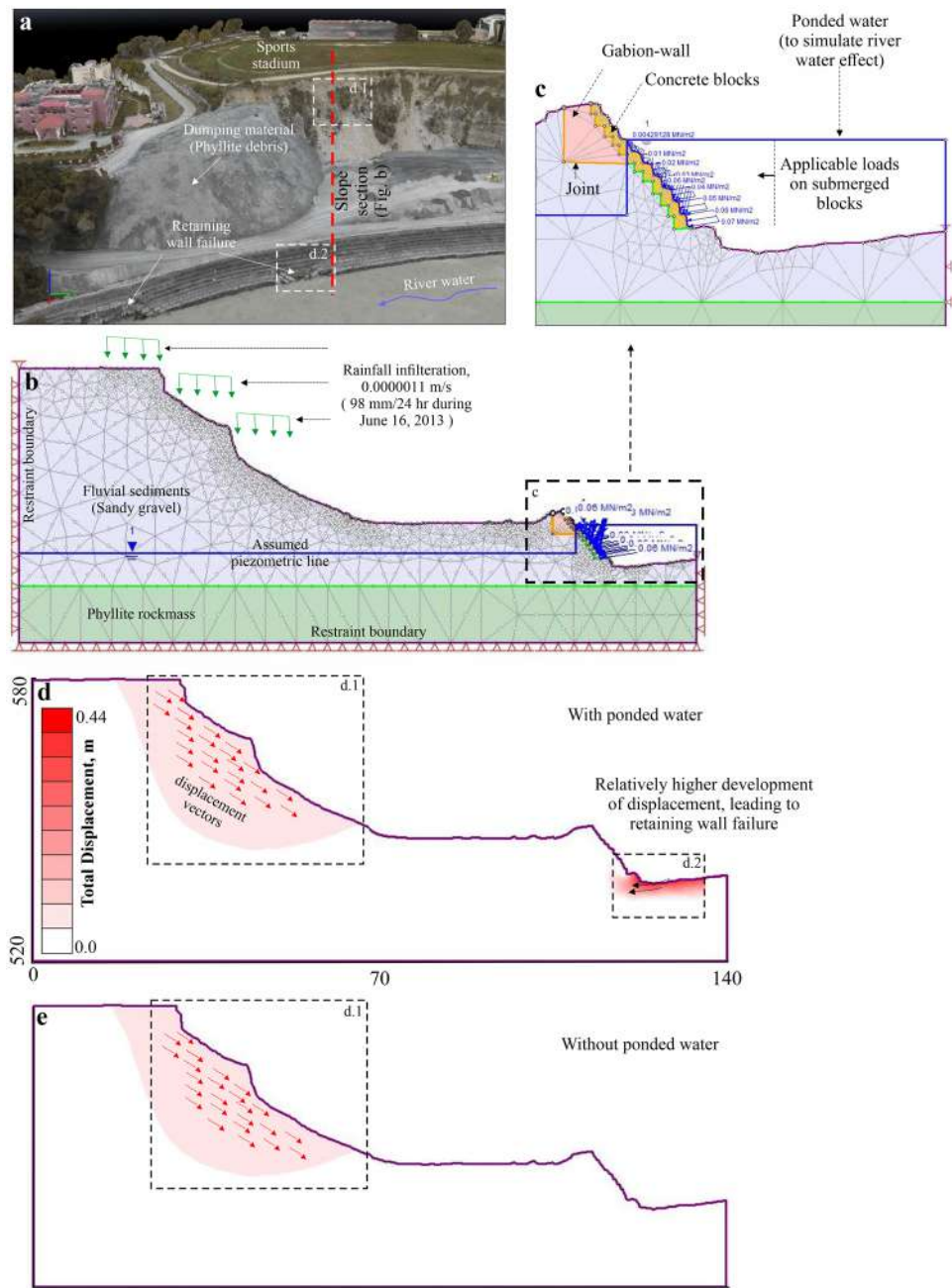
### Flood simulation

Since the study area has been subjected to floods in the past (Ziegler et al. 2014; Sundriyal et al. 2015), possibility of another similar or more impactful flood cannot be denied. Therefore, to determine the velocity and stream power of potential flood that might impact the riverbank slope and retaining wall, we performed a flood simulation with upper boundary at 330 MW Srinagar Hydroelectric project reservoir and a lower boundary 500 m downstream from the study area

(Fig. 3f–h). Notably, the unexpected release of water from this reservoir by dam authorities during the June 2013 flood has been attributed to a widespread socio-economic loss in the downstream region, and hence a monetary fine of 1.1 M USD was imposed on dam authorities by National Green Tribunal, India (<https://sandrp.in/tag/uttarakhand-floods-of-june-2013/>; <https://www.thehindu.com/sci-tech/energy-and-environment/notice-to-hydel-firm-over-damage-to-uttarakhand-town/article5620878.ece>, retrieved on 17/06/2022).

We used 2D unsteady shallow water equations (SWE) (Temam 1968). The formulation described below is a basis of flood simulation in the HEC-RAS (v.6.3.1), which is used in the present study by considering diffusion wave approximation. The formulation has the following assumptions: flow is incompressible, it has uniform density,

**Fig. 7** Slope stability analysis. **a** Highlighting the location of slope section used for slope stability analysis. Zones d.1 and d.2 represent exposed riverbank slope and collapsed retaining wall. **b** 2D slope section. Rainfall infiltration is based on June 16, 2013 rainfall event when slope saturated and was carved out by flood. **c** Zoomed section highlighting applicable loads on submerged blocks of retaining wall. **d, e** Total displacement pattern with water ponding and without water ponding



hydro-static pressure and equations are Reynold averaged to approximate turbulent motion, and the vertical length scale is much smaller than horizontal. Thus, the mass conservation equation for 2D-unsteady flow is

$$\frac{\partial h}{\partial t} + \frac{\partial Uh}{\partial x} + \frac{\partial Vh}{\partial y} = Q \tag{2}$$

Here,  $h$ , flow depth (m);  $U$  and  $V$ , velocity in  $x$  and  $y$  directions (m/s); and  $Q$ , discharge ( $m^3/s$ ).

When horizontal length  $>$  vertical length, volume conservation implies that  $V_z < V_{x,y}$ . Further, in absence of variable density,

wind friction (drag), Non-hydrostatic pressure, vertical average of momentum equation, is adequate. The SWE therefore achieves momentum conservation as follows:

$$\begin{aligned} \frac{\partial u}{\partial t} + u \frac{\partial u}{\partial x} + v \frac{\partial u}{\partial y} - f_c v = g \frac{\partial z_s}{\partial x} + \frac{1}{h} \frac{\partial}{\partial x} \left( v_{e_x} \cdot h \frac{\partial u}{\partial x} \right) \\ + \frac{1}{h} \frac{\partial}{\partial y} \left( v_{e_x} \cdot h \frac{\partial u}{\partial y} \right) - \frac{\tau_{bx}}{\rho R} \\ + \frac{\tau_{sx}}{\rho h} - (x \text{ direction}) \end{aligned} \tag{3}$$

$$\begin{aligned} \frac{\partial v}{\partial t} + u \frac{\partial v}{\partial x} + v \frac{\partial v}{\partial y} - f_c u = g \frac{\partial z_s}{\partial y} + \frac{1}{h} \frac{\partial}{\partial x} \left( v_{e_y} \cdot h \frac{\partial v}{\partial x} \right) \\ + \frac{1}{h} \frac{\partial}{\partial y} \left( v_{e_y} \cdot h \frac{\partial v}{\partial y} \right) - \frac{\tau_{by}}{\rho R} \\ + \frac{\tau_{sy}}{\rho h} - (\text{y direction}) \end{aligned} \quad (4)$$

Here,  $u$  and  $v$ , velocities in Cartesian coordinates;  $f_c$ , coriolis parameter ( $2\omega \sin \varphi$ ). Here,  $\varphi$  is latitude and  $\omega$  is angular velocity of earth;  $Z_s$ , water surface elevation;  $\tau_b$ , bottom shear stress;  $\tau_s$ , surface wind stress;  $R$ , hydraulic radius ( $A/w$ ).  $A$  represents cross sectional area of channel, and  $w$  represents wetted perimeter;  $v_e$ , eddy viscosity coefficient.

The bottom shear stress can be determined using the following equation:

$$\tau_b = \rho C_D |v|v \quad (5)$$

Here,  $v$  is flow velocity,  $\rho$ , water density;  $C_D$ , drag coefficient, which can be determined as

$$C_D = \frac{n^2 g}{R^{1/3}} \quad (6)$$

Here,  $n$ , Manning roughness coefficient. The “ $n$ ” can be calculated using the following equation (Jarrett 1985):

$$n = 0.39 S_f^{(0.38)} (R)^{-0.16} \quad (7)$$

Here,  $s_f$  is friction slope (or energy slope: slope of energy gradient). Once, “ $n$ ,”  $A$ ,  $S_f$ ,  $Q$  (flow discharge), and  $R$  parameters are known, the flow velocity can be calculated using the following equation:

$$Q = VA = (1/n)A.R^{2/3} \cdot \sqrt{S_f} \quad (8)$$

Similarly, once  $\tau_b$  is known, shear velocity can be determined using following equation:

$$u_s = \sqrt{\tau_b / \rho} \quad (9)$$

The region used for flood simulation, along with historical river discharge, is shown in Fig. 3. Flood was simulated at the following range of river discharge; 1500, 2000, 2500, 3000, 3500, and 4000 m<sup>3</sup>/s. The input parameters and their values used in the flood simulation are presented in Supplementary Table 3. Manning coefficient ( $n$ ) was taken in view of dominant grain size of river bed, i.e., gravely sand (Aldridge and Garrett 1973; Arcement and Schneider 1989). Turbulence coefficients were taken in view of gentle meanders and moderate surface irregularities (Supplementary Fig. 3).

## Results

### Slope stability evaluation

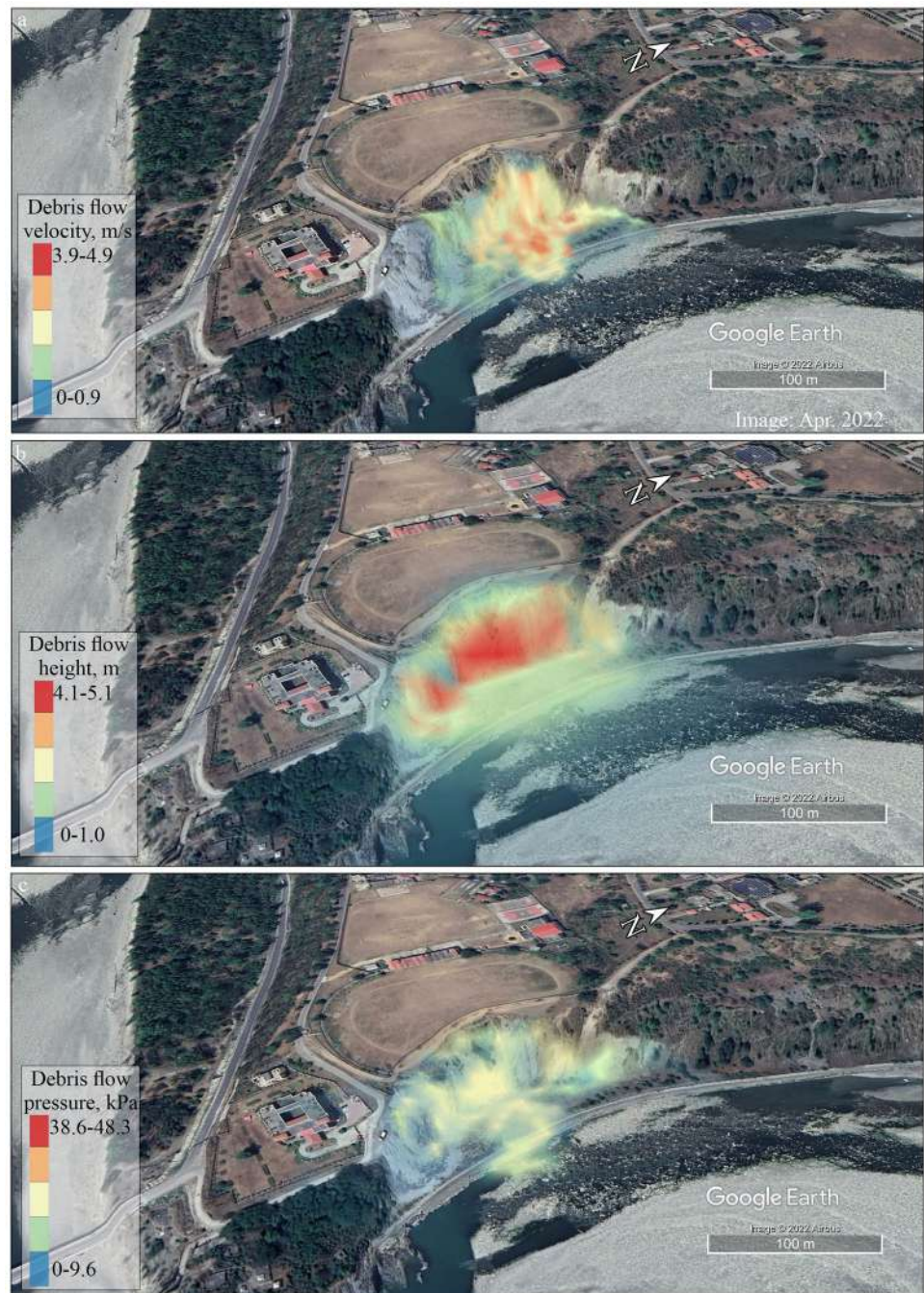
Static displacement (or equilibrium state) is shown in Supplementary Fig. 4. It is noted that during the water ponding, the riverbank toe (or slope toe) accommodating retaining wall develops relatively higher total displacement (0.1–0.4 m) and relatively lower (0.04–0.12 m) in the exposed fluvial sediments section highlighted as d.1 (Fig. 7d, e). The retaining wall failure at two places (marker d.2) can be attributed to this relatively higher total displacement at the riverbank toe. This can be further understood from the “water ponding effect.” In order to highlight the influence of water ponding, slope was also simulated without water ponding, which shows no displacement at the slope toe. Water ponding effect has been attributed to the lateral force of water that pushes embankments backward, and in the case of retaining wall along the water body, the backward rotation has also been noted (Nowatzki and Wrench 1988; Adair 2002; Hubble and Carli 2015). The displacement in the exposed fluvial section (marker d. 1) is an outcome of decreased shear strength, which refers to rainfall infiltration (based on maximum rainfall at this location, i.e., 98 mm/24 h.). The displacement vectors point toward the slope toe and hence may be responsible for the forward bulging of retaining wall. Further, to justify the selection of values of main input parameters, sensitivity analysis was performed (Supplementary Fig. 5). It is noted that angle of internal friction of soil and Poisson’s ratio have relatively more influence on displacement in this case study. Kumar et al. (2021b) have also noted the dominating influence of these parameters in case of debris laden hillslopes. The output of the values selected for the analysis remains in the middle of varying pattern. This exposed fluvial section, which develops slope instability under rainfall effect, is also prone to debris flow that is described below.

### Debris flow evaluation

Debris flow velocity ranges from 1 to 5 m/s along the riverbank slope with relatively higher values (3–5 m/s) in the central part (Fig. 8). Debris flow height ranges from 1 to 5 m with somewhat higher values in the central part, too. The impact pressure of debris flow ranges from 9.6 to 30 kPa, and it strikes the retaining wall with a pressure of 25–30 kPa (Fig. 8c).

Among all these parameters, flow velocity and flow pressure are noted to follow relatively better correlation (Fig. 9a–c). It implies that increasing debris flow velocity will result in increased debris flow pressure. Further, on

**Fig. 8** Debris flow results. **a–c** Debris flow velocity, height, and pressure. Results are based on depth of 5 m, density of  $1900 \text{ kg/m}^3$ , friction of 0.2, and turbulence of  $150 \text{ m/s}^2$



taking a range of input parameters, we noted that among all output variables (debris flow height, velocity, and pressure), pressure is relatively more sensitive to density, depth, and turbulence, whereas for friction, velocity and pressure are equally sensitive (Fig. 9d–o). Bugnion et al. (2012) and the reference therein have also noted such inter-dependency of flow velocity and pressure. Among all input parameters that were used for sensitivity, density is found to result in more scattering of pressure and

velocity (Fig. 9i). Such scattering effect caused by density variation can be understood from the Voellmy-Salm fluid flow continuum model (Voellmy 1955; Salm 1993). It assumes density as a primary component of formulation and its variation have considerable effect on velocity component, as can be seen in Eq. (1). However, it is noted that the pressure–velocity correlation fits relatively better until 6 m/s and 50 kPa and above these values, scattering takes place (Fig. 9c, f, i, l, o).

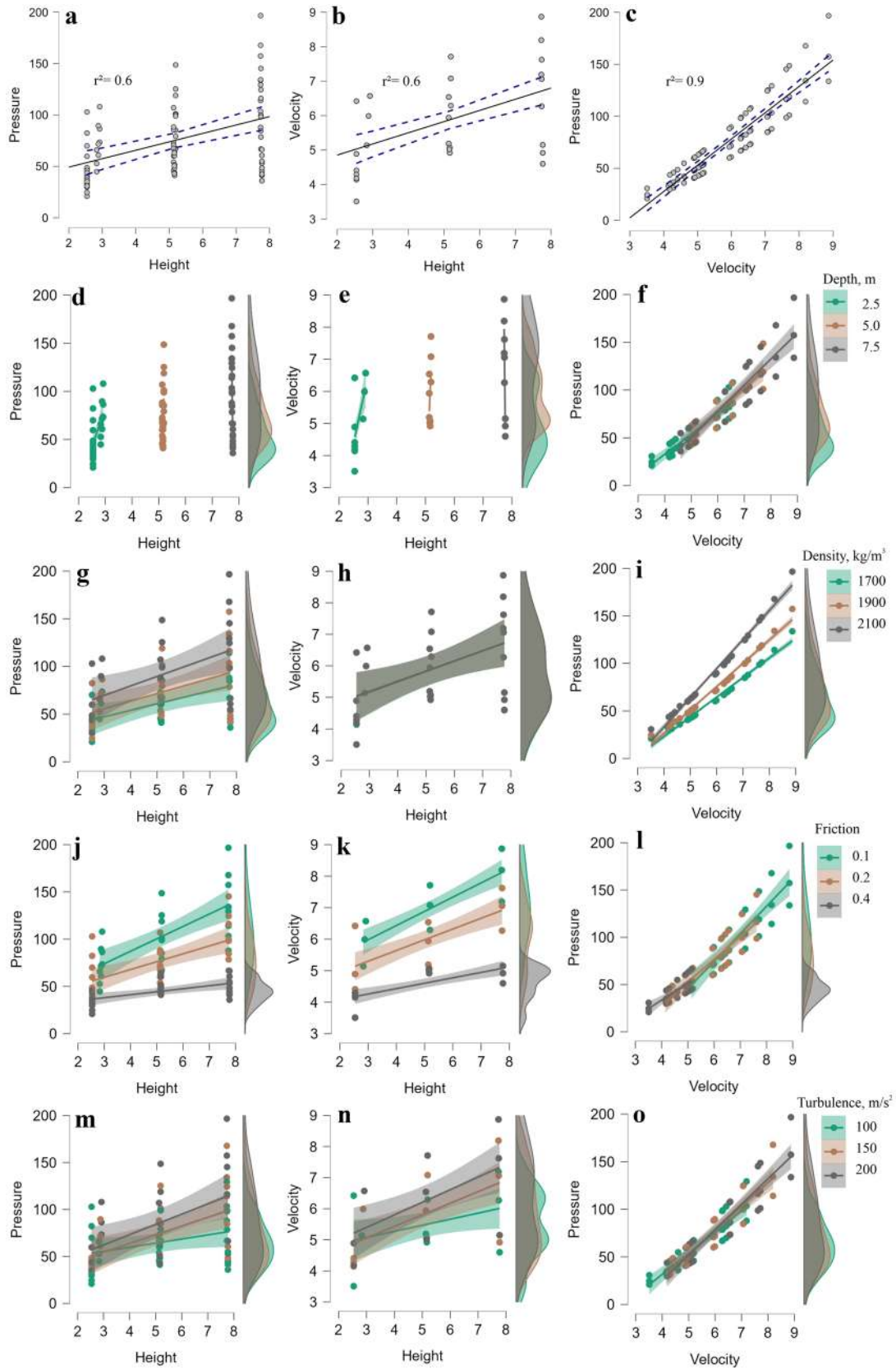


**Fig. 9** Debris flow sensitivity. **a–c** Correlation of debris flow height, velocity, and pressure. **d–f** Debris flow height, velocity, and pressure at varying depth. **g–i** Debris flow height, velocity, and pressure at varying density. **j–l** Debris flow height, velocity, and pressure at varying friction coefficient. **m–o** Debris flow height, velocity, and pressure at varying turbulence coefficient

## Flood impact evaluation

Potential flood in response to a maximum river discharge of  $1500 \text{ m}^3/\text{s}$  from the upstream HEP reservoir may pick up a velocity of 5–20 m/s (Fig. 10a, b). This velocity increases up to 10–15 m/s at the following two places between HEP reservoir and study area: the first corresponds to deep gorge just 300 m downstream from the reservoir and the second corresponds to study area (i.e., exposed riverbank slope). Further, such potential flood was also simulated at a range of river discharge ( $Q = 1500, 2000, 2500, 3000, 3500,$  and  $4000 \text{ m}^3/\text{s}$ ) to determine the flood velocity impact at the retaining wall. At this range of  $Q$ , flood velocity attains the peak ( $10 \pm 2 \text{ m/s}$ ) at the lower part along the retaining wall (section A–B) (Fig. 10c).

The flood stream power in response to a maximum river discharge of  $1500 \text{ m}^3/\text{s}$  from the upstream HEP reservoir ranges from 0.1 to 0.5 M N/ms with higher values confined to deep gorge just 300 m downstream from the reservoir (Fig. 10d, e). Along the riverbank (or retaining wall), it remains 0.1 M N/ms. Similar to flood velocity, flood stream power was also determined at a range of river discharge ( $Q = 1500, 2000, 2500, 3000, 3500,$  and  $4000 \text{ m}^3/\text{s}$ ). We noted that stream power also attains its peak with  $0.2 \pm 0.1 \text{ M N/ms}$  at the lower part along the retaining wall (section A–B) (Fig. 10f).

## Discussion

The study area and upstream catchment area have been subjected to floods/channel debris flows even in the past (Ziegler et al. 2014; Sundriyal et al. 2015; Srivastava et al. 2017; Rana et al. 2021), but the frequency of such events, including landslides, cloud bursts, and snow/rock avalanches, have increased in the past 10 years (Sundriyal et al. 2015; Rana et al. 2021). Frequent occurrence of these activities can be attributed to changing climate, as highlighted through rainfall, temperature, and runoff pattern (Fig. 2). Anthropogenic activities and the resultant change in land use/land cover might also have contributed to such change in climatic parameters in the upstream catchment (Joshimath, Badrinath, and Kedarnath regions) of the study area (Agarwal et al. 2022). However, anthropogenic activities are local in nature, whereas changing climate and resultant impacts are being observed in different parts of Himalaya and other mountains (Bhutiyan et al. 2010;

Shekhar et al. 2010). Therefore, it is more rational to relate the frequent occurrence of floods/channel debris flows to the changing climate, and the possibility of another such events in study area and upstream catchment cannot be denied. Though the floods had impacted the study area in the past, the extent of possible flood impacts was rarely studied. Therefore, the possible impacts of the potential flood were determined by using a range of river discharge as the main input, whereas flood velocity and stream power pattern were aimed as outputs (Fig. 10). Along with the flood impact, the stability of riverbank slope and its tendency as debris flow source were also evaluated that are being discussed first.

We found that the riverbank slope is unstable in nature as the material near the crown may displace forward  $\sim 0.12 \text{ m}$  under saturation (rainfall effect) and the slope toe accommodating retaining wall may displace  $\sim 0.4 \text{ m}$  under water ponding (Fig. 7). The forward displacement initiated at the top and displacement at slope toe might be major contributory factors in the retaining wall collapse at two places (Fig. 4b). In case of water ponding along the solid structures like retaining wall, the displacement or failure of retaining walls has been attributed to the backward rotation of such solid structures due to backward force of water body (Nowatzki and Wrench 1988; Adair 2002; Hubble and Carli 2015). Further, since the retaining wall is situated along the river channel, it straightens the river flow, increasing the water velocity and consequent bank/retaining wall erosion (Adair 2002). Apart from the forward displacement impact and backward water push, the retaining wall is also subjected to potential debris flow with a pressure of 25–30 kPa from the unstable riverbank slope in the central part (Fig. 8c). These relatively higher values of debris flow in the central part can be attributed to relatively steeper topography (Fig. 11a).

Such debris flow impact pressure may rise to higher values if we consider velocity-dependent empirical equations of debris flow impact pressure (Bugnion et al. 2012);  $p = c \cdot \rho \cdot v^2$  (where  $c$  is a coefficient that has been proposed by Swiss and Hong Kong guidelines (GEO Report 2000; Egli 2005) as 2–3,  $\rho$  is water density, and  $v$  is flow velocity). Using this equation with  $c$  as 2, range of  $v$  as 2–5 m/s, and  $\rho$  as  $1700\text{--}2000 \text{ kg/m}^3$ , debris flow impact pressure is noted to vary from 13.6 to 100 kPa. Further, if we consider  $c$  as 3, the upper limit of pressure might reach up to 150 kPa. Notably, the predicted pressure of 25–30 kPa and empirical equation based highest pressure will impact the retaining wall where it is already collapsed. Since the study area had received 148–150 mm of rainfall during June 16–17, 2013 flood and rainfall of this magnitude are becoming more frequent (Fig. 2g), and the possibility of saturation of unstable slope and resultant debris flow becomes more prevalent.

Further, though we have determined potential displacement contributed by rainfall infiltration in Fig. 7, the process

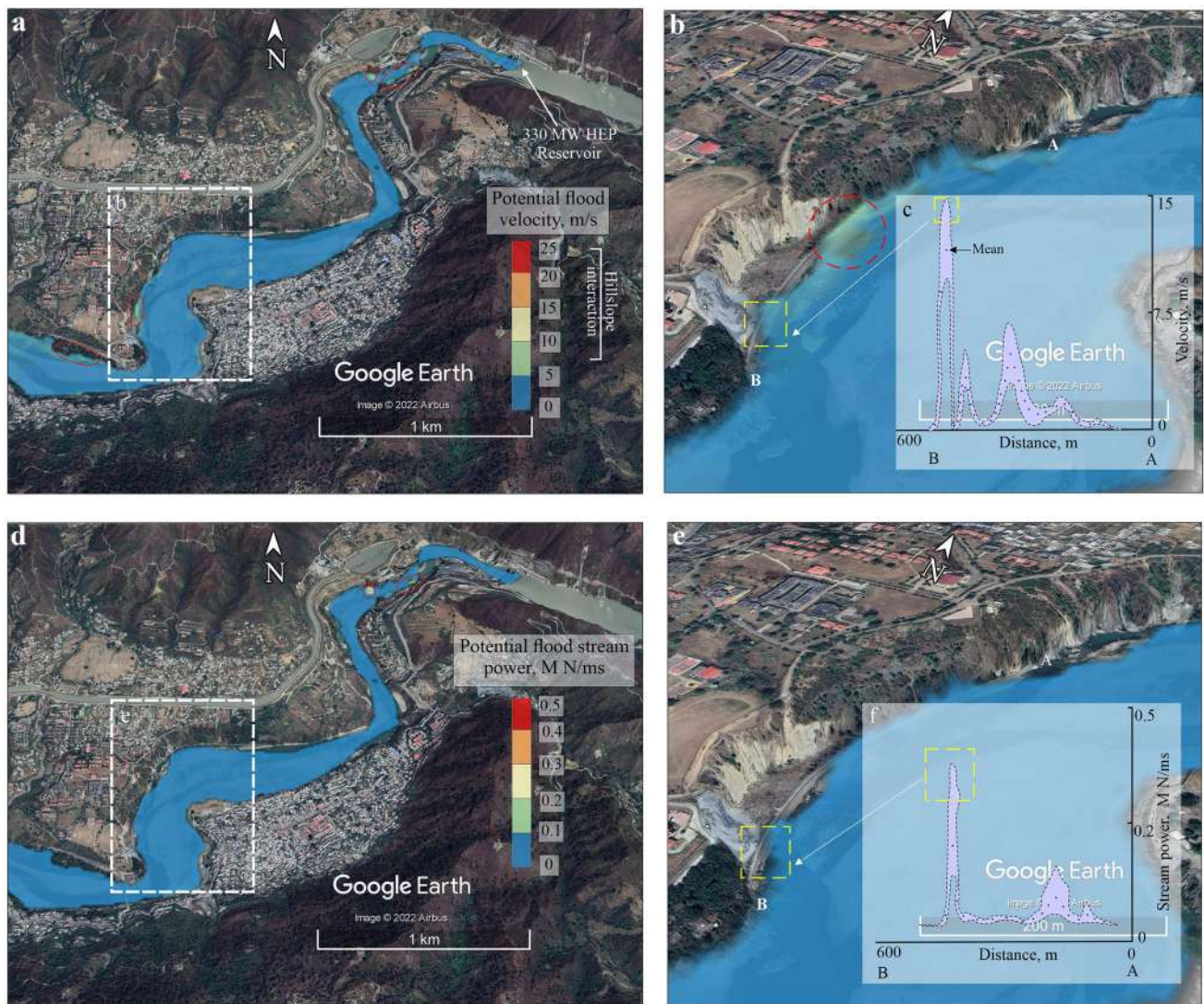


**Fig. 10** Flood simulation results. **a, b** Potential flood velocity. Red polygons highlight relatively higher values. **c** Potential flood velocity along the retaining wall (A–B) at a range of river discharge ( $Q = 1500, 2000, 2500, 3000, 3500,$  and  $4000 \text{ m}^3/\text{s}$ ). **d, e** Potential flood stream

power. **f** Potential flood stream power along the retaining wall (A–B) at a range of river discharge ( $Q = 1500, 2000, 2500, 3000, 3500,$  and  $4000 \text{ m}^3/\text{s}$ )

involving infiltration, saturation, resultant loss of shear strength, and potential failure needs to be addressed. In order to involve such saturation component in our slope model, we used Van Genuchten function (Van Genuchten 1980) as the soil water retention model. According to this model, matric suction has been observed to be more sensitive to rainfall as this process increases the pore water pressure and hence increases matric suction. Such increasing matric suction has been observed to increase the shear strength of soil up to a peak followed by a sharp decline in shear strength (Abd et al. 2020). In many case studies, this decrease in shear strength has led to the failure in soil mass (Fourie et al. 1999; Fredlund 2000).

Thus, the displacement caused by rainfall infiltration, as shown in Fig. 7, seems viable as laboratory-based studies,

mentioned above, have observed similar pattern of deformation during saturation. Notably, despite the frequent rainfall-induced landslides in the NW Himalaya, studies exploring the infiltration, subsequent saturation, and slope instability have been relatively rare (Singh et al. 2018; Thomas et al. 2023). A detailed explanation of such field and model-based hydrological perspectives along with monitoring can be accessed in similar case studies (Yang et al. 2019; Wei et al. 2020).

Furthermore, the retaining wall collapse that we have discussed in the context of instability of riverbank slope and potential debris flow owes this collapse/failure to nearby depressions in the river channel, too (Fig. 11). During floods, these depressions offer decreased hydraulic

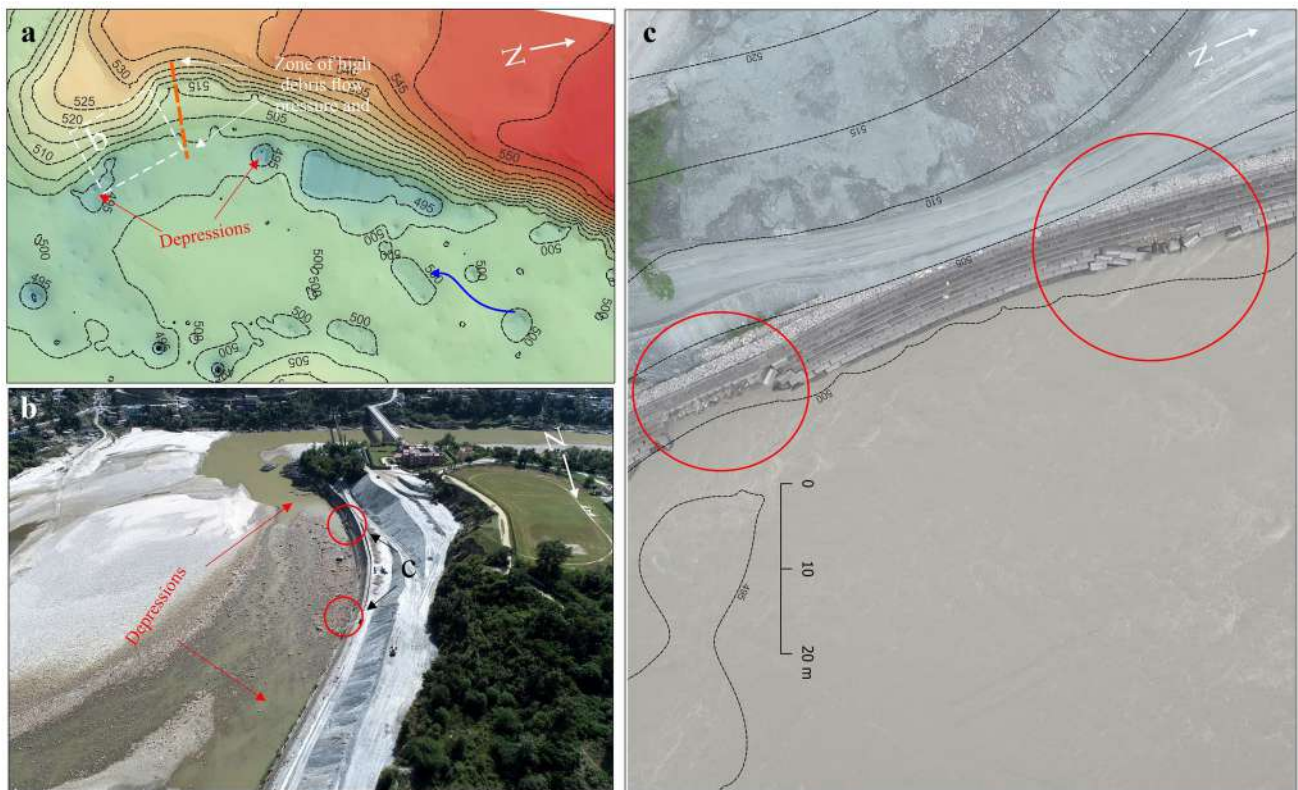


**Fig. 11** a–c Contour profiles in the study area. Red polygons in (b) highlight the retaining wall collapse. Source of contour: 0.5 m spatial resolution DTM, prepared using processing of DJI Phantom 4 RTK based images

radius in limited region that will increase the drag coefficient and slope friction of the river bed in that region and hence increased shear velocity as per shallow water equations (SWE) (Eqs. (5)–(9)). Such increased flow velocity has been observed to increase the erosion of riverbanks and/or the scouring of retaining walls (Nowatzki and Wrench 1988; Hubble and Carli 2015). Along with the implications of river channel depressions during a potential flood, the retaining wall will also be subjected to 10–15 m/s flood velocity and ~0.1 M N/ms flood stream power if considering peak river discharge as 1500 m<sup>3</sup>. These parameters may rise up to 10 ± 2 m/s and 0.2 ± 0.1 M N/ms at a range of river discharge ( $Q = 1500, 2000, 2500, 3000, 3500, \text{ and } 4000 \text{ m}^3/\text{s}$ ) (Fig. 10c, f). Notably, the reliability of these flood parameters mainly depends on river discharge, which was used in the present study based on historical river discharge patterns (Fig. 3b–e). Further, the river discharge during previous floods and similar studies in the upstream region of the study area has also been observed to range between 1500 and 1800 m<sup>3</sup>/s (Rao et al. 2014; Panwar et al. 2017).

Thus, if we summarize all the findings together, we observe that retaining wall protecting the riverbank slope might not sustain the pressure of potential debris flow and/or

flood, particularly at the places where it is already collapsed (Fig. 12). Further, another factor that might contribute to the slope instability and increased load on retaining wall,

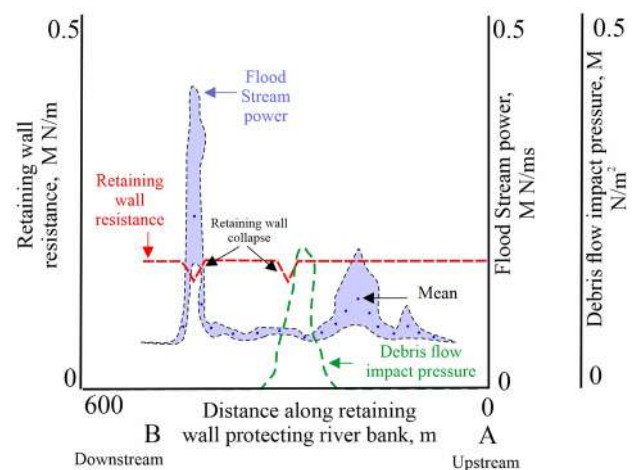


**Fig. 12** Retaining wall resistance vs. forces of debris flow and flood. A–B sections can also be seen in Fig. 10(b) and (e). Retaining wall resistance is explained in the “Fieldwork, laboratory analyses, and unmanned air vehicle (UAV) mapping” section. The value of debris flow pressure corresponds to 150 kPa (maximum possible debris flow pressure as mentioned in the “Discussion” section)

in case of saturation is dumping of phyllitic rock fragments on this riverbank slope (Fig. 7a). Such dumping has been taking place since July 2022 and may aggravate the already weakened slope and retaining wall, as also observed in other case studies (Satyanaga et al. 2020).

## Conclusion

The study area and upstream catchment area have been subjected to frequent hydro-climatic events in the past, but the frequency of such events has increased in the last decade that is attributed to changing climatic. Thus, the possibility of another such event in the study area and upstream catchment cannot be denied. We found that the retaining wall, which has already collapsed at two places in the last 3–4 years under the normal flow of river water, is subjected to local and regional impacts that might damage it completely and hence making the riverbank slope and roads/other infrastructure (buildings), situated above, vulnerable again.

The local impacts involve instability of this riverbank slope and potential debris flow. The slope material near the crown may displace forward  $\sim 0.12$  m under saturation (rain-fall effect), and the slope toe accommodating retaining wall may displace  $\sim 0.4$  m under water ponding. The potential debris flow of this unstable mass from the slope may impact the retaining wall with a pressure of 25–30 kPa that might increase up to 150 kPa if we consider flow velocity-dependent empirical equations. The regional impact involves the influence of flood velocity and stream power as the retaining wall will also be subjected to 10–15 m/s flood velocity and  $\sim 0.1$  M N/ms flood stream power if consider peak river discharge as  $1500 \text{ m}^3$ . These parameters may further rise up to  $10 \pm 2$  m/s and  $0.2 \pm 0.1$  M N/ms at a range of river discharge ( $Q = 1500, 2000, 2500, 3000, 3500, \text{ and } 4000 \text{ m}^3/\text{s}$ ).

Since the study area had received 148–150 mm of rainfall during June 2013 flood and rainfall of such magnitudes are becoming more frequent, the possibility of debris flow is becoming prevalent in the slope. The upstream catchment that has become the source of frequent disastrous floods in the last decade has been experiencing frequent snow avalanches/rock avalanches since the year 2021, and such events pose more risk in downstream regions. This study is an attempt to identify the possible response of the riverbank slope and/or retaining wall in case of another disastrous flood/debris flow that might put the lives and infrastructure of the study area at risk.

**Supplementary Information** The online version contains supplementary material available at <https://doi.org/10.1007/s10064-023-03205-4>.

**Acknowledgements** Authors are thankful for the financial support by the Department of Science and Technology, Government of India, New Delhi [Ref. No. DST/CCP/MRDP/187/2019(G)]. We also acknowledge

constructive comments/suggestions of editor-in-chief (Prof. Louis N.Y. Wong), editor (Prof. Jia-Wen Zhou), and three anonymous reviewers.

**Author contribution** YS, VK, DSB, and NR conceived the idea. VK, SK, and NC performed the field work and collected soil samples. VK, SK, NC, NR, and FK performed UAV mapping. VK and YP processed the UAV imagery. MKP performed the laboratory analysis. VK performed the numerical simulations. All authors contributed to the writing of the final draft.

**Funding** Authors are thankful for the financial support by the Department of Science and Technology, Government of India, New Delhi [Ref. No. DST/CCP/MRDP/187/2019(G)].

**Data availability** Though the majority of the dataset has been presented as supplementary, additional dataset may be provided on request.

## Declarations

**Competing interests** The authors declare no competing interests.

## References

- Abd IA, Fattah MY, Mekkiyah H (2020) Relationship between the matric suction and the shear strength in unsaturated soil. *Case Studi Constr Mater* 13:e00441
- Adair SE (2002) Management and techniques for riparian restorations: roads field guide. US Department of Agriculture, Forest Service, Rocky Mountain Research Station
- Agarwal S, Kumar V, Kumar S, Sundriyal Y, Bagri DS, Chauhan N, Rana N (2022) Identifying potential hotspots of land use/land cover change in the last 3 decades, Uttarakhand, NW Himalaya. <https://doi.org/10.31223/X5VK9F> (Preprint)
- Alcrudo F (2002) A state of the art review on mathematical modelling of flood propagation. First IMPACT project Workshop, Wallingford, UK
- Aldridge BN, Garrett JM (1973) Roughness coefficients for stream channels in Arizona. US Department of the Interior, US Geological Survey
- Arcement GJ, Schneider VR (1989) Guide for selecting Manning's roughness coefficients for natural channels and flood plains. U.S. Department of Transportation, Federal Highway Administration
- Baker VR (1987) Paleoflood hydrology and extraordinary flood events. *J Hydrol* 96(1–4):79–99
- Barton NR, Bandis SC (1990) Review of predictive capabilities of JRC-JCS model in engineering practice. In: Barton N, Stephansson O (eds) *Rock joints*. Rotterdam, pp 603–610
- Barton N, Choubey V (1977) The shear strength of rock joints in theory and practice. *Rock Mech* 10(1–2):1–54
- Bhutiyan MR, Kale VS, Pawar NJ (2010) Climate change and the precipitation variations in the northwestern Himalaya: 1866–2006. *Int J Climatol J R Meteorol Soc* 30(4):535–548
- Begueria S, Van Asch TW, Malet JP, Gröndahl S (2009) A GIS-based numerical model for simulating the kinematics of mud and debris flows over complex terrain. *Nat Hazards and Earth Syst Sci* 9(6):1897–909
- Bilham R (2019) Himalayan earthquakes: a review of historical seismicity and early 21st century slip potential. *Geol Soc London Spec Publ* 483(1):423–482
- Bugnion L, McArdell BW, Bartelt P, Wendeler C (2012) Measurements of hillslope debris flow impact pressure on obstacles. *Landslides* 9(2):179–187

- Chopra R (2014) Uttarakhand: development and ecological sustainability. Oxfam India, New Delhi
- Christen M, Kowalski J, Bartelt P (2010a) RAMMS: numerical simulation of dense snow avalanches in three-dimensional terrain. *Cold Reg Sci Technol* 63(1–2):1–14
- Coulomb CA (1776) An attempt to apply the rules of maxima and minima to several problems of stability related to architecture. *Mém Acad R Sci* 7:343–382
- Das R, Samanta G (2022) Impact of floods and river-bank erosion on the riverine people in Manikchak block of Malda district, West Bengal. *Environ Dev Sustain* 1–23
- Dhakal S (2014) Flood hazard in Nepal and new approach of risk reduction. *Int J Landslide Environ* 1(1):13–14
- Dimri AP, Choudhary A, Kumar D (2020) Elevation dependent warming over Indian Himalayan region. Himalayan weather and climate and their impact on the environment. Springer, Cham, pp 141–156
- Dimri AP, Allen S, Huggel C, Mal S, Ballesteros-Canovas JA, Rohrer M, Pandey A (2021) Climate change, cryosphere and impacts in the Indian Himalayan Region. *Curr Sci* 120(5):774–790
- Egli T (2005) *Wegleitung Objektschutz gegen gravitative naturgefahren*. VKF
- Fourie AB, Rowe D, Blight GE (1999) The effect of infiltration on the stability of the slopes of a dry ash dump. *Geotechnique* 49(1):1–13
- Fredlund DG (2000) The 1999 R.M. Hardy Lecture: the implementation of unsaturated soil mechanics into geotechnical engineering. *Can Geotech J* 37:963–986
- Gadgil S, Rajeevan M, Francis PA (2007) Monsoon variability: Links to major oscillations over the equatorial Pacific and Indian oceans. *J Curr Sci* 93(2):182–194
- GEO Report (2000) Review of Natural Terrain Landslide Debris-resisting Barrier Design. No. 104, Hong Kong. [https://www.cedd.gov.hk/eng/publications/geo/geo-reports/geo\\_rpt104/index.html](https://www.cedd.gov.hk/eng/publications/geo/geo-reports/geo_rpt104/index.html)
- Godt JW, Coe JA (2007) Alpine debris flows triggered by a 28 July 1999 thunderstorm in the central Front Range, Colorado. *Geomorphology* 84(1–2):80–97
- Goldsmith W, Gray D, McCullah J (2013) Bioengineering case studies: sustainable stream bank and slope stabilization. Springer Science & Business Media
- Gray DH, Sotir RB (1996) Biotechnical and soil bioengineering slope stabilization: a practical guide for erosion control. John Wiley & Sons
- Griffiths DV, Lane PA (1999) Slope stability analysis by finite elements. *Geotechnique* 49(3):387–403
- Gupta V, Jamir I, Kumar V, Devi M (2017) Geomechanical characterisation of slopes for assessing rockfall hazards in the Upper Yamuna Valley, Northwest Higher Himalaya, India. *Himal Geol* 38(2):156–170
- Hoek E, Kaiser PK, Bawden WF (1995) Support of underground excavations in hard rock. A. A. Balkema, Rotterdam
- Hubble TCT, De Carli E (2015) Mechanisms and processes of the millennium drought river bank failures: Lower Murray River, South Australia. Goyder Institute for Water Research (Technical Report)
- Huffman GJ, Bolvin DT, Braithwaite D, Hsu KL, Joyce RJ, Kidd C, Xie P (2020) Integrated multi-satellite retrievals for the global precipitation measurement (GPM) mission (IMERG). Satellite precipitation measurement. Springer, Cham, pp 343–353
- Hunt KMR, Curio J, Turner AG, Schiemann R (2018) Subtropical westerly jet influence on occurrence of western disturbances and Tibetan Plateau vortices. *Geophys Res Lett* 45(16):8629–8636
- Hürlimann M, Rickenmann D, Medina V, Bateman A (2008) Evaluation of approaches to calculate debris-flow parameters for hazard assessment. *Eng Geol* 102:152–163
- IRC: Indian Road Congress (2018) Guidelines for design and Installation of Gabion Structures, SP 116. Bureau of Indian Standards, Delhi, India. <https://archive.org/details/gov.in.irc.sp.116.2018>
- Jamir I, Gupta V, Kumar V, Thong GT (2017) Evaluation of potential surface instability using finite element method in Kharsali Village, Yamuna Valley, Northwest Himalaya. *J Mt Sci* 14(8):1666–1676
- Jarrett RD (1985) Determination of roughness coefficients for streams in Colorado, vol 85. US Department of the Interior Geological Survey
- Jing L (2003) A review of techniques, advances and outstanding issues in numerical modelling for rock mechanics and rock engineering. *Int J Rock Mech Min Sci* 40(3):283–353
- Kayal JR (1996) Precursor seismicity, foreshocks and aftershocks of the Uttarkashi earthquake of October 20, 1991 at Garhwal Himalaya. *Tectonophysics* 263(1–4):339–345
- Kumar A, Gupta AK, Bhambri R, Verma A, Tiwari SK, Asthana AKL (2018) Assessment and review of hydrometeorological aspects for cloudburst and flash flood events in the third pole region (Indian Himalaya). *Polar Sci* 18:5–20
- Kumar V, Cauchie L, Mreyen AS, Micu M, Havenith HB (2021a) Evaluating landslide response in a seismic and rainfall regime: a case study from the SE Carpathians, Romania. *Nat Hazard* 21(12):3767–3788
- Kumar V, Jamir I, Gupta V, Bhasin RK (2021b) Inferring potential landslide damming using slope stability, geomorphic constraints, and run-out analysis: a case study from the NW Himalaya. *Earth Surf Dyn* 9(2):351–377
- Martha TR, Roy P, Govindharaj KB, Kumar KV, Diwakar PG, Dadhwal VK (2015) Landslides triggered by the June 2013 extreme rainfall event in parts of Uttarakhand state, India. *Landslides* 12(1):135–146
- McNally A (2018) NASA/GSFC/HSL, FLDAS Noah Land Surface Model L4 Global Monthly 0.1 x 0.1 degree (MERRA-2 and CHIRPS), Greenbelt, MD, USA, Goddard Earth Sciences Data and Information Services Center (GES DISC). <https://doi.org/10.5067/5NHC22T9375G>. Accessed 2 Apr 2022
- Mohr O (1914) *Abhandlungen aus dem Gebiete der Technischen Mechanik*, 2nd edn. Ernst, Berlin
- Nowatzki EA, Wrench BP (1988) Geotechnical investigation into causes of failure of a Gabion retaining wall. International conference on case histories in geotechnical engineering. Missouri University of Science and Technology, pp 1477–1481
- O'Brien JS, Julien PY, Fullerton WT (1993) Two-dimensional water flood and mudflow simulation. *J Hydraul Eng* 119(2):244–61
- Pandey Y, Dharmaraju R, Chauhan PKS (2001) Estimation of source parameters of Chamoli Earthquake, India. *J Earth Syst Sci* 110(2):171–177
- Panwar S, Agarwal V, Chakrapani GJ (2017) Morphometric and sediment source characterization of the Alaknanda river basin, headwaters of river Ganga, India. *Nat Hazards* 87(3):1649–1671
- Pudasaini SP, Mergili M (2019) A multi-phase mass flow model. *J Geophys Res Earth Surf* 124(12):2920–42
- Rajeevan M, Francis PA (2007) Monsoon variability: links to major oscillations over the equatorial Pacific and Indian oceans. *Curr Sci* 93(2):182–194
- Rana N, Sundriyal Y, Sharma S, Khan F, Kaushik S, Chand P, Juyal N (2021) Hydrological characteristics of 7th February 2021 Rishi Ganga flood: implication towards understanding flood hazards in higher Himalaya. *J Geol Soc India* 97(8):827–835
- Rao KD, Rao VV, Dadhwal VK, Diwakar PG (2014) Kedarnath flash floods: a hydrological and hydraulic simulation study. *Curr Sci* 106:598–603
- Rickenmann D (2005) Runout prediction methods. Debris-flow hazards and related phenomena. Springer, Berlin, Heidelberg, pp 305–324
- Rickenmann D, Scheidl C (2013) Debris-flow runout and deposition on the fan. In: Schneuwly-Bollschweiler M et al (eds) Dating torrential processes on fans and cones. Advances in global change research, vol 47. Springer, Dordrecht. <https://doi.org/10.1007/978-94-007-4336-65>

- Salm B (1993) Flow, flow transition and runout distances of flowing avalanches. *Ann Glaciol* 18:221–226
- Sati VP, Kumar S (2022) Environmental and economic impact of cloudburst-triggered debris flows and flash floods in Uttarakhand Himalaya: a case study. *Geoenviron Disasters* 9(1):1–11
- Satyanaga A, Rahardjo H, Leong EC, Chia YH, Wang JY (2020) Effect of dual-porosity material on stability of slope during rainfall. *Unsaturated soils: research & applications*. CRC Press, pp 1227–1233
- Schroth MH, Istok JD, Selker JS, Oostrom M, White MD (1998) Multifluid flow in bedded porous media: laboratory experiments and numerical simulations. *Adv Water Resour* 22(2):169–183
- Shekhar MS, Chand H, Kumar S, Srinivasan K, Ganju A (2010) Climate-change studies in the western Himalaya. *Ann Glaciol* 51(54):105–112
- Singh AK, Kundu J, Sarkar K (2018) Stability analysis of a recurring soil slope failure along NH-5, Himachal Himalaya, India. *Nat Hazards* 90:863–885
- Srivastava P, Kumar A, Chaudhary S, Meena N, Sundriyal YP, Rawat S, Ziegler AD (2017) Paleofloods records in Himalaya. *Geomorphology* 284:17–30
- Sundriyal Y, Kumar V, Chauhan N, Kaushik S, Ranjan R, Punia MK (2023) Brief communication on the NW Himalayan towns; slipping towards potential disaster. *Nat Hazards Earth Syst Sci* 1–9. <https://doi.org/10.5194/nhess-2022-296>,
- Sundriyal YP, Shukla AD, Rana N, Jayangondaperumal R, Srivastava P, Chamyal LS, Juyal N (2015) Terrain response to the extreme rainfall event of June 2013: evidence from the Alaknanda and Mandakini River Valleys, Garhwal Himalaya, India. *Episodes J Int Geosci* 38(3):179–188
- Temam R (1968) Une méthode d'approximation de la solution des équations de Navier-Stokes. *Bull Soc Math France* 96:115–152
- Teng J, Jakeman AJ, Vaze J, Croke BF, Dutta D, Kim SJEM (2017) Flood inundation modelling: a review of methods, recent advances and uncertainty analysis. *Environ Model Softw* 90:201–216
- Thomas J, Gupta M, Prusty G (2023) Assessing global parameters of slope stability model using earth data observations for forecasting rainfall-induced shallow landslides. *J Appl Geophys* 212:104994
- Thorne CR, Tovey NK (1981) Stability of composite river banks. *Earth Surf Proc Land* 6(5):469–484
- Van der Wal M (2020) Bank protection structures along the Brahmaputra-Jamuna River, a study of flow slides. *Water* 12(9):2588
- Van Genuchten MTh (1980) A closed form equation for predicting the hydraulic conductivity of unsaturated soils. *Soil Sci Soc Am J* 44:892–898
- Voellmy A (1955) On the destructive force of avalanche, translation No. 2. *Avalanche Study Center, United States Department of Agriculture, USA*. <https://collections.lib.utah.edu/ark:/87278/s6sq8xc1>. Accessed 2 Apr 2022
- Wei X, Fan W, Cao Y, Chai X, Bordoni M, Meisina C, Li J (2020) Integrated experiments on field monitoring and hydro-mechanical modeling for determination of a triggering threshold of rainfall-induced shallow landslides. A case study in Ren River catchment, China. *Bull Eng Geol Env* 79:513–532
- Yang Z, Cai H, Shao W, Huang D, Uchimura T, Lei X, Qiao J (2019) Clarifying the hydrological mechanisms and thresholds for rainfall-induced landslide: in situ monitoring of big data to unsaturated slope stability analysis. *Bull Eng Geol Env* 78:2139–2150
- Ziegler AD, Wasson RJ, Bhardwaj A, Sundriyal YP, Sati SP, Juyal N, Saklani U (2014) Pilgrims, progress, and the political economy of disaster preparedness—the example of the 2013 Uttarakhand flood and Kedarnath disaster. *Hydrol Process* 28(24):5985–5990

Springer Nature or its licensor (e.g. a society or other partner) holds exclusive rights to this article under a publishing agreement with the author(s) or other rightsholder(s); author self-archiving of the accepted manuscript version of this article is solely governed by the terms of such publishing agreement and applicable law.